Identification of DAXX As A Restriction Factor Of SARS-CoV-2 Through A CRISPR/Cas9 Screen

Alice Mac Kain[1,2], Ghizlane Maarifi[3], Sophie-Marie Aicher[2,4], Nathalie Arhel[3], Artem Baidaliuk[5], Thomas Vallet[1], Quang Dinh Tran[1,2], Alexandra Hardy[1], Maxime Chazal[4], Françoise Porrot[6], Molly OhAinle[7], Jared Carlson-Stevermer[8], Jennifer Oki[8], Kevin Holden[8], Etienne Simon-Lorière[5], Timothée Bruel[6], Olivier Schwartz[6], Nolwenn Jouvenet[4], Sébastien Nisole[3], Marco Vignuzzi[$1], Ferdinand Roesch*[1,9]

Author Affiliations:

1 Viral populations and pathogenesis, Institut Pasteur, CNRS UMR 3569, F-75015 Paris, France
2 Université de Paris, F-75013 Paris, France
3 Institut de Recherche en Infectiologie de Montpellier (IRIM), Université de Montpellier, CNRS, 34090 Montpellier, France
4 Virus sensing and signaling, Institut Pasteur, CNRS UMR 3569, F-75015 Paris, France
5 Evolutionary genomics of RNA viruses, Institut Pasteur, F-75015 Paris, France
6 Virus and Immunity, Institut Pasteur, CNRS UMR 3569, F-75015 Paris, France
7 Divisions of Human Biology, Fred Hutchinson Cancer Research Center, Seattle, United States
8 Synthego Corporation, 3565 Haven Avenue, Menlo Park, CA 94025
9 UMR 1282 ISP, INRAE Centre Val de Loire, Nouzilly, France

*** Corresponding author:**

Ferdinand Roesch.
ORCID: 0000-0003-0702-7778
Email: ferdinand.roesch@inrae.fr
Phone: +33 2 47 42 79 15
Current address: Equipe 3IMo ; UMR 1282 ISP - Infectiologie et Santé Publique
Centre de recherche INRAE Val de Loire
Route de Crotelles 37380 Nouzilly, France

$ Co-corresponding author:

Marco Vignuzzi
ORCID: 0000-0002-4400-771X
Email: marco.vignuzzi@pasteur.fr
Phone: 33 1 4568 8242

Abstract:

While interferon restricts SARS-CoV-2 replication in cell culture, only a handful of Interferon Stimulated Genes with antiviral activity against SARS-CoV-2 have been identified. Here, we describe a functional CRISPR/Cas9 screen aiming at identifying SARS-CoV-2 restriction factors. We identified DAXX, a scaffold protein residing in PML nuclear bodies known to limit the replication of DNA viruses and retroviruses, as a potent inhibitor of SARS-CoV-2 replication in human cells. Basal expression of DAXX was sufficient to limit the replication of the virus, and DAXX over-expression further restricted infection. In contrast with most of its previously described antiviral activities, DAXX-mediated restriction of SARS-CoV-2 was independent of the SUMOylation pathway. SARS-CoV-2 infection triggered the re-localization of DAXX to cytoplasmic sites of viral replication and led to its degradation. Together, these results demonstrate that DAXX is a potent restriction factor for SARS-CoV-2 and that the virus has evolved a mechanism to counteract its action.

Introduction. Severe Acute Respiratory Syndrome Coronavirus 2 (SARS-CoV-2) is the causative agent of COVID-19 and the third coronavirus to cause severe disease in humans after the emergence of SARS-CoV in 2002 and Middle East Respiratory Syndrome-related Coronavirus (MERS-CoV) in 2012. Since the beginning of the pandemic, SARS-CoV-2 has infected more than 140 million people and claimed 3 million lives. While the majority of infected individuals experience mild (or no) symptoms, severe forms of COVID-19 are associated with respiratory failure, shock and pneumonia. Innate immune responses play a key role in COVID-19 pathogenesis: immune exhaustion (1) and reduced levels of type-I and type-III interferon (IFN) have been observed in the plasma of severe COVID-19 patients (2,3). Imbalanced immune responses to SARS-CoV-2, with a low and delayed IFN response coupled to early and elevated levels of inflammation, have been proposed to be a major driver of COVID-19 (4,5). Neutralizing auto-antibodies against type-I IFN (6) and genetic alterations in several IFN pathway genes (7) have also been detected in critically ill COVID-19 patients. These studies highlight the crucial need to characterize the molecular mechanisms by which IFN pathway effectors may succeed, or fail, to control SARS-CoV-2 infection.

Although SARS-CoV-2 has been described to antagonize the IFN pathway by different mechanisms involving the viral proteins ORF3b, ORF9b ORF6, and nsp15 (8), detection of SARS-CoV-2 by the innate immune sensor Mda5 (9,10) leads to the synthesis of IFN and expression of IFN Stimulated Genes (ISGs) in human airway epithelial cells (4). IFN strongly inhibits SARS-CoV-2 replication when added in cell culture prior to infection (11,12) or when administered intranasally in hamsters (13), suggesting that some ISGs might have antiviral activity (14). However, relatively few ISGs with antiviral activity against SARS-CoV-2 have been identified so far. For instance, spike-mediated viral entry and fusion is restricted by LY6E (15,16) and IFITMs (17,18). Mucins have also been suggested in a recent pre-print to restrict viral entry (19). ZAP, which targets CpG dinucleotides in RNA viruses, also restricts SARS-CoV-2, albeit moderately (20). A recent overexpression screen identified 65 ISGs as potential inhibitors of SARS-CoV-2 (21), and found that BST-2/Tetherin is able to restrict viral budding, although this activity is counteracted by the viral protein ORF7a. The RNA helicase DDX42 was also shown to restrict several RNA viruses, including SARS-CoV-2 (22). We hypothesize that additional ISGs with antiviral activity against SARS-CoV-2 remain to be discovered. Other antiviral factors that are not induced by IFN may also inhibit SARS-CoV-2. While several whole-genome CRISPR/Cas9 screens identified host factors required for SARS-CoV-2 replication (23–28), none focused on antiviral genes.

Here, we performed a CRISPR/Cas9 screen designed to identify restriction factors for SARS-CoV-2, assessing the ability of 1905 ISGs to modulate SARS-CoV-2 replication in human epithelial lung cells. We report that the Death domain-associated protein 6 (DAXX), a scaffold protein residing in PML nuclear bodies (29) and restricting DNA viruses (30) and retroviruses (31,32), is a potent inhibitor of SARS-CoV-2 replication. SARS-CoV-2 restriction by DAXX is largely independent of the action of IFN, and unlike most of its other known activities, of the SUMOylation pathway. Within hours of infection, DAXX re-localizes to sites of viral replication in the cytoplasm, likely targeting viral

transcription. We also show that during the course of SARS-CoV-2 infection, DAXX is degraded, suggesting that SARS-CoV-2 developed a mechanism to counteract DAXX restriction.

Results.

A restriction factor-focused CRISPR/Cas9 screen identifies genes potentially involved in SARS-CoV-2 inhibition. To identify restriction factors limiting SARS-CoV-2 replication, we generated a pool of A549-ACE2 cells knocked-out (KO) for 1905 potential ISGs, using the sgRNA library we previously developed to screen HIV-1 restriction factors (33). This library includes more ISGs than most published libraries, as the inclusion criteria was less stringent (fold-change in gene expression in THP1 cells, primary CD4+ T cells or PBMCs $\geq$ 2). Transduced cells were selected by puromycin treatment, treated with IFNα and infected with SARS-CoV-2. Infected cells were immuno-labelled with a spike (S)-specific antibody and analyzed by flow cytometry. As expected (11,12), IFNα inhibited infection by 7-fold (**Fig. S1**). Infected cells were sorted based on S expression (**Fig. 1a**), and DNA was extracted from infected and non-infected control cells. Integrated sgRNA sequences in each cell fraction were amplified by PCR and sequenced by NGS. Statistical analyses using the MAGeCK package (34) led to the identification of sgRNAs significantly enriched or depleted in infected cells representing antiviral and proviral factors, respectively (**Fig. 1b**). Although our screen was not designed to explicitly study proviral factors, we did successfully identify the well-described SARS-CoV-2 co-factor cathepsin L (CTSL) (35), validating our approach. USP18, a negative regulator of the IFN signaling pathway (36), and ISG15, which favors Hepatitis C Virus replication (37), were also identified as proviral ISGs. In contrast, core IFN pathway genes such as the IFN receptor (IFNAR1), STAT1, and STAT2, were detected as antiviral factors, further validating our screening strategy. LY6E, a previously described inhibitor of SARS-CoV-2 entry (15,16), was also a significant hit. Moreover, our screen identified APOL6, IFI6, DAXX and HERC5, genes that are known to encode proteins with antiviral activity against other viruses (38–41), but had not previously been identified in the context of SARS-CoV-2 infection. For all these genes except APOL6, individual sgRNAs were consistently enriched (for antiviral factors) or depleted (for proviral factors) in the sorted population of infected cells, while non-targeting sgRNAs were not (**Fig. 1c**).

LY6E and DAXX display antiviral activity against SARS-CoV-2. To validate the ability of the identified hits to modulate SARS-CoV-2 replication in human cells, we generated pools of A549-ACE2 knocked-out (KO) cells for different genes of interest by electroporating a mix of 3 sgRNA/Cas9 ribonucleoprotein (RNP) complexes per gene target. Levels of gene editing were above 80% in all of the A549-ACE2 KO cell lines, as assessed by sequencing of the edited *loci* (**Table 1**). As controls, we used cells KO for IFNAR1, for the proviral factor CTSL or for the antiviral factor LY6E, as well as cells electroporated with non-targeting (NTC) sgRNAs/Cas9 RNPs. These different cell lines were then treated with IFNα and infected with SARS-CoV-2. Viral replication was assessed by measuring the levels of viral RNA in the supernatant of infected cells using RT-qPCR (**Fig. 2a**). In parallel, we titrated the levels of infectious viral particles released into the supernatant of infected cells (**Fig. 2b**). As expected, infection was significantly reduced in CTSL KO cells, confirming the proviral effect of this gene (35). Among the selected antiviral candidate genes, only 2 had a significant impact on SARS-CoV-2 replication: LY6E, and to an even greater degree, DAXX. Both genes restricted replication in absence of IFNα, an effect which was detectable at the level of viral RNA (8-fold and 42-fold reduction of infection, respectively, **Fig. 2a**) and of infectious virus (15-fold and 62-fold reduction, **Fig. 2b**). Based on available single-cell RNAseq datasets (42), DAXX is expected to be expressed in cell types relevant for SARS-CoV-2 such as lung epithelial cells, macrophages and T cells (**Fig. S3**).

In IFNα-treated cells. DAXX and LY6E KO led to a modest, but significant rescue of viral replication, which was particularly visible when measuring the levels of infectious virus by plaque assay titration (**Fig. 2b**), while the antiviral effect of IFNα treatment was completely abrogated in IFNAR1 KO cells, as expected (**Fig. 2c**). However, IFNα still had a strong antiviral effect on SARS-CoV-2 replication in both DAXX KO and LY6E KO cells (**Fig. 2c**). While DAXX and LY6E contribute to

the IFN-mediated restriction, this suggests that there are likely other ISGs contributing to this effect. Although DAXX is sometimes referred to as an ISG, its expression is only weakly induced by IFN in some human cell types (31,43). Consistent with this, we found little to no increase in DAXX expression in IFNα-treated A549-ACE2 cells (**Fig. S2**). In addition, we tested the antiviral effect of DAXX on several SARS-CoV-2 variants that have been suggested in a recent report to be partially resistant to the antiviral effect of IFN (44). In these experiments, the 20I/501Y.V1 (UK), together with the 20J/501Y.V3 (Brazil) variant, were indeed less sensitive to IFN. DAXX, however, restricted all variants to a similar level than the historical strain of SARS-CoV-2 (**Fig. 2d**). This suggest that while some variants may have evolved towards IFN-resistance, they are still efficiently restricted by DAXX.

To further validate the antiviral activity of DAXX against SARS-CoV-2, we quantified the levels of several viral transcripts in WT and DAXX KO cells (**Fig. 2e**). The levels of all the transcripts tested strongly increased in DAXX KO cells (20 to 30-fold across all experiments). This further confirmed that DAXX strongly interferes with SARS-CoV-2 replication and suggests that it may target viral transcription, or an earlier step of the viral life cycle.

DAXX restriction is SUMO-independent. DAXX is a small scaffold protein that acts by recruiting other SUMOylated proteins in nuclear bodies through its C-terminal SUMO-Interacting Motif (SIM) domain (45). The recruitment of these factors is required for the effect of DAXX on various cellular processes such as transcription and apoptosis, and on its antiviral activities (31,46–48). DAXX can also be SUMOylated itself (49), which may be important for some of its functions. To investigate the role of SUMOylation in DAXX-mediated SARS-CoV-2 restriction, we used overexpression assays to compare the antiviral activity of DAXX WT with two previously described DAXX mutants (50). First, we used a version of DAXX in which 15 lysine residues have been mutated to arginine (DAXX 15KR), which is unable to be SUMOylated; and second, a truncated version of DAXX that is missing its C-terminal SIM domain (DAXXΔSIM) (47) and is unable to interact with its SUMOylated partners. A549-ACE2 were refractory to SARS-CoV-2 infection upon transfection with any plasmid, precluding us from using this cell line. Instead, we transfected 293T-ACE2 cells, another SARS-CoV-2 permissive cell line (18). Western blot (**Fig. S4a**) and flow cytometry (**Fig. S4b**) analyses showed that DAXX WT and mutants were expressed to similar levels, with a transfection efficiency of 40 to 50% for all three constructs.

We examined the effect of DAXX WT overexpression on the replication of SARS-CoV-2-mNeonGreen (51) by microscopy. DAXX overexpression starkly reduced the number of infected cells (**Fig. 3a**), revealing that DAXX-mediated restriction is not specific to A549-ACE2 cells. Using double staining for HA-tagged DAXX and SARS-CoV-2, we found that most of the DAXX-transfected cells were negative for infection, and conversely, that most of the infected cells did not express transfected DAXX (**Fig. 3a**), indicating that DAXX imposes a major block to SARS-CoV-2 infection.

In order to quantify the antiviral effect of overexpressed DAXX WT and mutants, we assessed the number of cells positive for the S protein (among transfected cells) by flow cytometry (**Fig. 3c-d**) and the abundance of viral transcripts by qRT-PCR (**Fig. S4c**). DAXX WT, 15KR and ΔSIM all efficiently restricted SARS-CoV-2 replication. Indeed, at 24 hours p.i., the proportion of infected cells (among HA-positive cells) was reduced by 2 to 3-fold as compared to control transfected cells for all 3 constructs (**Fig. 3c**). This effect was less pronounced but still significant at 48 hours p.i. (**Fig. 3d**). Moreover, DAXX overexpression led to a significant reduction of the levels of two different viral transcripts (**Fig. S4c**), in line with our earlier results showing that DAXX targets viral transcription (**Fig. 2e**). Together, these results show that DAXX overexpression restricts SARS-CoV-2 transcription in a SUMOylation-independent mechanism.

SARS-CoV-2 infection triggers DAXX re-localization and degradation. DAXX mostly localizes in nuclear bodies (29), whereas SARS-CoV-2 replication occurs in the cytoplasm. We reasoned that DAXX localization may be altered during the course of infection in order for the restriction factor to exert its antiviral effect. To test this hypothesis, we infected 293T-ACE2 cells with SARS-CoV-2 and used high-resolution confocal microscopy to study the localization of endogenous DAXX (**Fig. 4**). As expected (29), DAXX mostly localizes in the nuclei of non-infected cells, forming discrete *foci*. 6h after

SARS-CoV-2 infection, DAXX begins to re-localize to the cytoplasm, although nuclear *foci* can still be detected. At 24h post-infection, however, DAXX is completely depleted from nuclear bodies, and is found almost exclusively in the cytoplasm of infected cells, in close association with SARS-CoV-2 dsRNA. Western blot analysis revealed that SARS-CoV-2 infection induces a marked decrease of total DAXX expression in infected cells (**Fig. 5a**). This effect is visible at MOI 0.1, and almost complete DAXX degradation can be observed at MOI 1. These results suggest that DAXX may be actively targeted by SARS-CoV-2 for degradation during the course of infection. SARS-CoV-2 papain-like protease (PLpro) is a possible candidate for this function, as it cleaves ISG15 from Mda5 (52) and IRF3 (53). It was also shown that foot-and-mouth disease virus (FDMV) PLpro degrades DAXX (54). We treated cells with GRL-0617, an inhibitor of SARS-CoV-2 PLpro (53). Strikingly, GRL-0617 treatment partially restores DAXX expression (**Fig. 5a**) and subcellular localization to nuclear bodies in infected cells at 24h p.i. at MOI 0.1 (**Fig. 5b**). Although we cannot exclude that GRL-0617 treatment may have an indirect effect on DAXX levels by inhibiting SARS-CoV-2 replication itself, this is unlikely to be a major mitigating effect at 24h post-infection, particularly since imaging analysis reveals a restoration of DAXX specifically in SARS-CoV-2 infected cells (**Fig. 5b**). Further work will be required to uncover whether PLPro or a proteolytic product of the viral polyprotein chain degrades DAXX.

Discussion.

Comparison with other screens. The whole-genome CRISPR/Cas9 screens conducted to date on SARS-CoV-2 infected cells mostly identified host factors necessary for viral replication (23–28) and did not focus on antiviral genes, as did our screen. Two overexpression screens, however, identified ISGs with antiviral activity against SARS-CoV-2 (16,21). In the first one, Pfaender *et al.* screened 386 ISGs for their antiviral activity against the endemic human coronavirus 229E, and identified LY6E as a restriction factor inhibiting both 229E and SARS-CoV-2. Our screen also identified LY6E as a top hit (**Fig.1**), further validating the findings of both studies. Four additional genes had significant p-values in both Pfaender *et al.* and our work: IFI6, HERC5, OAS2 and SPSB1 (**Table S5-S6**). We showed that knocking-out LY6E and DAXX only partially rescued SARS-CoV-2 replication in IFN-treated cells (**Fig. 2)**, suggesting that they contribute modestly to IFN-mediated restriction and that other IFN effectors active against SARS-CoV-2 remain to be identified. For instance, other ISGs, such as IFITMs, inhibit SARS-CoV-2 viral entry (17–19). In the second screen, Martin Sancho *et al.* tested 399 ISGs against SARS-CoV-2. Among the 65 antiviral ISGs identified, they focused on BST-2/Tetherin, that targets viral budding. BST-2/Tetherin was not a significant hit in our screen (**Table S5-6**). This discrepancy can be easily explained by the fact that our screen relies on the sorting of S-positive cells, and is therefore unable to detect late-acting antiviral factors. Of note, DAXX was absent from the ISG libraries used by both overexpression screens, which explains why it was not previously identified as an antiviral ISG for SARS-CoV-2. In contrast, our sgRNA library, by including 1905 genes, targeted a wider set of ISGs and “ISG-like” genes, including genes like DAXX that are not (or only weakly) induced by IFN in some cell types (31,43). Interestingly, IFN has a stronger effect on DAXX expression levels in other mammals, including in some bat species (55). Future studies may investigate whether DAXX orthologs of different species are also able to restrict SARS-CoV-2 and whether DAXX participates in IFN-mediated viral restriction in these hosts.

DAXX is a restriction factor for SARS-CoV-2. Our CRISPR/Cas9 screen identifies DAXX as a potent antiviral factor restricting the replication of SARS-CoV-2, acting independently of IFN and likely targeting an early step of the viral life cycle such as transcription. DAXX fulfills all of the criteria defining a *bona fide* SARS-CoV-2 restriction factor: knocking-out endogenous DAXX leads to an enhanced viral replication (**Fig. 2**), while over-expression of DAXX restricts infection (**Fig. 3**). DAXX co-localizes with viral dsRNA (**Fig. 4**) and SARS-CoV-2 antagonizes DAXX to some degree, as evidenced by the degradation of DAXX induced by viral replication (**Fig. 5**). Although DAXX expression is not upregulated by IFN (**Fig. S2**), basal levels of expression are sufficient for its antiviral activity, as has been shown for other potent restriction factors. Single-cell RNAseq analyses (**Fig. S3**)

indicated that DAXX is expressed in cell types targeted by the virus in patients, such as lung epithelial cells and macrophages.

Mechanism of DAXX-mediated restriction. DAXX is mostly known for its antiviral activity against DNA viruses replicating in the nucleus, such as adenovirus 5 (AdV5) (56) and human papillomavirus (HPV) (57). Most of these viruses antagonize PML and/or DAXX, which interacts with PML in nuclear bodies (29). We show here that DAXX is also able to restrict a positive sense RNA virus that replicates in the cytoplasm, which may represent a first step into establishing DAXX as a broad-spectrum restriction factor. Recent studies have shown that DAXX inhibits the reverse transcription of HIV-1 in the cytoplasm (31,32). Within hours of infection, DAXX subcellular localization was altered, with DAXX accumulating in the cytoplasm and colocalizing with incoming HIV-1 capsids (32). Here, we observed a similar phenomenon, with a rapid re-localization of DAXX from the nucleus to viral replication sites (**Fig. 4**), where it likely exerts its antiviral effect. Early events in the replication cycle of both HIV-1 and SARS-CoV-2, such as viral fusion or virus-induced stress, may thus trigger DAXX re-localization to the cytoplasm. DAXX seems to inhibit SARS-CoV-2, however, by a distinct mechanism: whereas the recruitment of SUMOylated partners through the SIM-domain is required for the effect of DAXX on HIV-1 reverse transcription (31), it was not the case in the context of SARS-CoV-2 restriction. This result was surprising, since DAXX has no enzymatic activity and rather acts as a scaffold protein recruiting SUMOylated partners through its SIM domain (50). Some DAXX functions, such as interaction with the chromatin remodeler ATRX (29), are however SIM-independent. Future work should determine which DAXX domains and residues are required for its antiviral activity.

Antagonism of DAXX by SARS-CoV-2. SARS-CoV-2 replication triggers DAXX degradation (**Fig. 5**), which likely represents an efficient antagonism strategy. Other viruses are also able to degrade DAXX: for instance, the AdV5 viral protein E1B-55K targets DAXX for proteasomal degradation (56), and FDMV PLpro directly degrades DAXX (54). We speculate that the SARS-CoV-2 proteases PLpro or 3C-like proteinase might be involved. Treatment of cells with GRL-0617, an inhibitor of PLpro, partially prevented virus-induced DAXX degradation and restored DAXX localization to the nucleus. However, this effect could be indirect, since GRL-0617 also blocks SARS-CoV-2 replication by preventing polyprotein cleavage. Future work will be necessary to formally demonstrate the direct degradation of DAXX by PLpro and to determine whether other viral strategies promote evasion from DAXX restriction.

Material & Methods.

Cells, viruses & plasmids. HEK 293T (ATCC #CRL-11268) were cultured in MEM (Gibco #11095080) complemented with 10% FBS (Gibco #A3160801) and 2 mM L-Glutamine (Gibco # 25030081). VeroE6 (ATCC #CRL-1586), A549 (ATCC #CCL-185) and HEK 293T, both overexpressing the ACE2 receptor (A549-ACE2 and HEK 293T-ACE2, respectively), were grown in DMEM (Gibco #31966021) supplemented with 10% FBS (Gibco #A3160801), and penicillin/streptomycin (100 U/mL and 100 µg/mL, Gibco # 15140122). Blasticidin (10 µg/mL, Sigma-Aldrich #SBR00022-10ML) was added for selection of A549-ACE2 and HEK 293T-ACE2. All cells were maintained at 37°C in a 5% CO_2 atmosphere. Universal Type I Interferon Alpha (PBL Assay Science #11200-2) was diluted in sterile-filtered PBS 1% BSA according to the activity reported by the manufacturer. The strains BetaCoV/France/IDF0372/2020 (historical); hCoV-19/France/IDF-IPP11324/2020 (20I/501Y.V1 or UK); and hCoV-19/France/PDL-IPP01065/2021 (20H/501Y.V2 or SA) were supplied by the National Reference Centre for Respiratory Viruses hosted by Institut Pasteur and headed by Pr. Sylvie van der Werf. The human samples from which the historical, UK and SA strains were isolated were provided by Dr. X. Lescure and Pr. Y. Yazdanpanah from the Bichat Hospital, Paris, France; Dr. Besson J., Bioliance Laboratory, saint-Herblain France; Dr. Vincent Foissaud, HIA Percy, Clamart, France, respectively. These strains were supplied through the European Virus Archive goes Global (Evag) platform, a project that has received funding from the European Union's Horizon 2020 research and innovation programme under grant agreement #653316. The hCoV-19/Japan/TY7-501/2021 strain (20J/501Y.V3 or Brazil) was kindly provided by Jessica Vanhomwegen (Cellule d'Intervention Biologique d'Urgence; Institut Pasteur). The mNeonGreen reporter SARS-CoV-2 was provided by Pei-Yong Shi (51). Viral stocks were generated by infecting VeroE6 cells (MOI 0.01, harvesting at 3 dpi) using DMEM supplemented with 2% FBS and 1 µg/mL TPCK-trypsin (Sigma-Aldrich #1426-100MG). The Human Interferon-Stimulated Gene

CRISPR Knockout Library was a gift from Michael Emerman and is available on Addgene (Pooled Library #125753). The plentiCRISPRv.2 backbone was ordered through Addgene (Plasmid #52961). pMD2.G and psPAX2 were gifts from Didier Trono (Addgene #12259; #12260). pcDNA3.1 was purchased from Invitrogen. Plasmids constructs expressing WT and mutant HA-tagged DAXX constructs were kindly provided by Hsiu-Ming Shih (50).

Antibodies. For Western Blot, we used mouse anti-DAXX (diluted 1:1000, Abnova #7A11), rat anti-HA clone 3F10 (diluted 1:3000, Roche #11867423001) and mouse anti-GAPDH clone 6C5 (diluted 1:3000, Millipore #FCMAB252F). Secondary antibodies were goat anti-mouse and anti-rabbit HRP-conjugates (diluted 1:5000, GE Healthcare #NA931V and #NA934V). For immunofluorescence, we used rabbit anti-DAXX (diluted 1:50, Proteintech #20489-1-AP) and mouse anti-dsRNA J2 (diluted 1:50, Scicons #10010200). Secondary antibodies were goat anti-rabbit AF555 and anti-mouse AF488 (diluted 1:1000, ThermoFisher #A-21428 and #A-28175). For flow sorting of infected cells, we used the anti-S2 H2 162 antibody (diluted 1:150), a kind gift from Dr. Hugo Mouquet, (Institut Pasteur, Paris, France). Secondary antibody was donkey anti-mouse AF647 (diluted 1:1000, Invitrogen #A31571). For FACS analysis, we used rat anti-HA clone 3F10 (diluted 1:100, Sigma #2158167001) and mouse anti-dsRNA J2 (diluted 1:500, Scicons #10010200). Secondary antibodies were goat anti-rat AF647 and anti-mouse AF488 (diluted 1:1000, ThermoFisher #A-21247 #A-28175).

Generation of CRISPR/Cas9 library cells. HEK 293T cells were transfected with the sgRNA library plasmid together with plasmids coding for Gag/Pol (R8.2) and for the VSVg envelope (pVSVg) using a ratio of 5:5:1 and calcium phosphate transfection. Supernatants were harvested at 36h and 48h, concentrated 80-fold by ultracentrifugation (22,000 g, 4°C for 1h) and pooled. To generate ISG KO library cells, $36x10^6$ A549-ACE2 cells were seeded in 6 well plates (10^6 cells per well) 24h before transduction. For each well, 100 µL of concentrated lentivector was diluted in 500 µL of serum-free DMEM, supplemented with 10 µg/mL of DEAE dextran (Sigma #D9885). After 48h, transduced cells were selected by puromycin treatment for 20 days (1 µg/mL; Sigma #P8833).

CRISPR/Cas9 screen. $4x10^7$ A549-ACE2 cells were treated with IFNα (200U/mL). 16h later, cells were infected at a MOI of 1 in serum-free media complemented with TPCK-trypsin and IFNα (200 U/mL). After 90 min, the viral inoculum was removed, and cells were maintained in DMEM containing 5% FBS and IFNα (200 U/mL). After 24h, cells were harvested and fixed for 15 min in Formalin 1%. Fixed cells were washed in cold FACS buffer containing PBS, 2% Bovine Serum Albumin (Sigma-Aldrich #A2153-100G), 2 mM EDTA (Invitrogen #15575-038) and 0.1% Saponin (Sigma-Aldrich #S7900-100G). Cells were incubated for 30 min at 4°C under rotation with primary antibody diluted in FACS buffer. Incubation with the secondary antibody was performed during 30 min at 4°C under rotation. Stained cells were resuspended in cold sorting buffer containing PBS, 2% FBS, 25 mM Hepes (Sigma-Aldrich #H0887-100ML) and 5 mM EDTA. Infected cells were sorted on a BD FACS Aria Fusion. Sorted and control (non-infected, not IFN-treated) cells were centrifugated (20 min, 2,000g) and resuspended in lysis buffer (NaCl 300 mM, SDS 0.1%, EDTA 10 mM, EGTA 20 mM, Tris 10 mM) supplemented with 1% Proteinase K (Qiagen #19133) and 1% RNAse A/T1 (ThermoFisher #EN0551) and incubated overnight at 65°C. Two consecutive phenol-chloroform (Sigma #P3803-100ML) extractions were performed and DNA was recovered by ethanol precipitation. Nested PCR was performed using the Herculase II Fusion DNA Polymerase (Agilent, #600679) and the DNA oligos indicated in **Table S1**. PCR1 products were purified using QIAquick PCR Purification kit (Qiagen #28104). PCR2 products were purified using Agencourt AMPure XP Beads (Beckman Coulter Life Sciences #A63880). DNA concentration was determined using Qubit dsDNA HS Assay Kit (Thermo Fisher #Q32854) and adjusted to 2 nM prior to sequencing. NGS was performed using the NextSeq 500/550 High Output Kit v2.5 75 cycles (Illumina #20024906).

Screen analysis. Reads were demultiplexed using bcl2fastq Conversion Software v2.20 (Illumina) and fastx_toolkit v0.0.13. Sequencing adapters were removed using cutadapt v1.9.1 (58). The reference library was built using bowtie2 v2.2.9 (59). Read mapping was performed with bowtie2 allowing 1 seed mismatch in --local mode and samtools v1.9 (60). Mapping analysis and gene selection were performed using MAGeCK v0.5.6, normalizing the data with default parameters. sgRNA and gene enrichment analyses are available in **Table S5-S6**, respectively and full MAGeCK output at https://github.com/Simon-LoriereLab/crispr_isg_sarscov2.

Generation of multi-guide gene knockout cells. 3 sgRNAs per gene were designed (**Table S2**). 10 pmol of NLS-Sp.Cas9-NLS (SpCas9) nuclease (Aldevron #9212) was combined with 30 pmol total synthetic sgRNA (10 pmol for each sgRNA) (Synthego) to form RNPs in 20 µL total volume with SE Buffer (Lonza #V5SC-1002). The reaction was incubated at room temperature for 10 min. $2x10^5$ cells per condition were pelleted by centrifugation

at 100*g* for 3 min, resuspended in SE buffer and diluted to $2x10^4$ cells/µL. 5 µL of cell solution was added to the pre-formed RNP solution and gently mixed. Nucleofections were performed on a Lonza HT 384-well nucleofector system (Lonza #AAU-1001) using program CM-120. Immediately following nucleofection, each reaction was transferred to a 96-well plate containing 200 µL of DMEM 10% FBS ($5x10^4$ cells per well). Two days post-nucleofection, DNA was extracted using DNA QuickExtract (Lucigen #QE09050). Cells were lysed in 50 µL of QuickExtract solution and incubated at 68°C for 15 min followed by 95°C for 10 min. Amplicons were generated by PCR amplification using NEBNext polymerase (NEB #M0541) or AmpliTaq Gold 360 polymerase (ThermoFisher #4398881) and the primers indicated in **Table S3**. PCR products were cleaned-up and analyzed by Sanger sequencing. Sanger data files and sgRNA target sequences were input into Inference of CRISPR Edits (ICE) analysis https://ice.synthego.com/#/ to determine editing efficiency and to quantify generated indels (61). Percentage of alleles edited is expressed as an ice-d score.

SARS-CoV-2 infection assays. A549-ACE2 cells were infected by incubating the virus for 1h with the cells maintained in DMEM supplemented with 1 µg/ml TPCK-trypsin (Sigma #4370285). The viral input was then removed and cells were kept in DMEM supplemented with 2% FBS. For 293T-ACE2 cells, infections were performed without TPCK-trypsin. All experiments involving infectious material were performed in Biosafety Level 3 facilities in compliance with Institut Pasteur's guidelines and procedures.

Hit validation. $2.5x10^4$ A549-ACE2 KO cells were seeded in 96-well plates 18h before the experiment. Cells were treated with IFNα and infected as described above. At 72h post-infection, supernatants and cellular monolayers were harvested in order to perform qRT-PCR and plaque assay titration. Infectious supernatants were heat-inactivated at 80°C for 10 min. For intracellular RNA, cells were lysed in a mixture of Trizol Reagent (Invitrogen #15596018) and PBS at a ratio of 3:1. Total RNA was extracted using the Direct-zol 96 RNA kit (Zymo Research #R2056) or the Direct-zol RNA Miniprep kit (Zymo Research #R2050). qRT-PCR was performed either directly on the inactivated supernatants or on extracted RNA using the Luna Universal One-Step RT-qPCR Kit (NEB #E3005E) in a QuantStudio 6 thermocycler (Applied Biosystems) or in a StepOne Plus thermocycler (Applied Biosystems). Primers used are described in **Table S4**. Cycling conditions were the following: 10 min at 55°C, 1 min at 95°C and 40 cycles of 95°C for 10s and 60°C for 1 min. Results are expressed as PFU equivalents/mL as the standard curve was performed by diluting RNA extracted from a viral stock with a known titer. For plaque assay titration, VeroE6 cells were seeded in 24-well plates (10^5 cells per well) and infected with serial dilutions of infectious supernatant diluted in DMEM during 1h at 37°C. After infection, 0.1% agarose semi-solid overlays were added. At 72h post-infection, cells were fixed with Formalin 4% (Sigma #HT501128-4L) and plaques were visualized using crystal violet coloration.

Overexpression assay. $2x10^5$ 293T-ACE2 cells were seeded in a 24-well plate 18h before experiment. Cells were transfected with 500 ng of plasmids expressing HA-DAXX WT, HA-DAXX 15KR and HA-DAXXΔSIM plasmids, using Fugene 6 (Promega # E2691), following the manufacturer's instructions. HA-NRB1 was used as negative control. After 24h cells were infected at the indicated MOI in DMEM 2% FBS. When indicated, cells were treated with 10 mM of remdesivir (MedChemExpress #HY-104077) at the time of infection. For flow cytometry analysis, cells were fixed with 4% formaldehyde and permeabilized in a PBS 1% BSA 0.025% saponin solution for 30 min prior to staining with corresponding antibodies for 1h at 4°C diluted in the permeabilization solution. Samples were acquired on a BD LSR Fortessa and analyzed using FlowJo. Total RNA was extracted using a RNeasy Mini kit and submitted to DNase treatment (Qiagen). RNA concentration and purity were evaluated by spectrophotometry (NanoDrop 2000c, ThermoFisher). In addition, 500 ng of RNA were reverse transcribed with both oligo dT and random primers, using a PrimeScript RT Reagent Kit (Takara Bio) in a 10 mL reaction. Real-time PCR reactions were performed in duplicate using Takyon ROX SYBR MasterMix blue dTTP (Eurogentec) on an Applied Biosystems QuantStudio 5 (ThermoFisher). Transcripts were quantified using the following program: 3 min at 95°C followed by 35 cycles of 15s at 95°C, 20s at 60°C, and 20s at 72°C. Values for each transcript were normalized to expression levels of RPL13A. The primers used are indicated in **Table S4**.

Western blot. Cell lysates were prepared using RIPA lysis and extraction buffer (ThermoFisher #89901). Protein concentration was determined using Bradford quantification. Proteins were denaturated using 4X Bolt LDS Sample Buffer (Invitrogen) and 10X Bolt Sample Reducing Agent (Invitrogen). 40 µg of proteins were separated on Bolt 4-12% Bis-Tris Mini Protein Gels (Invitrogen) and transferred on membranes using the iBlot Transfer Stack PVDF mini (Invitrogen) and an iBlot Dry Blotting System (Invitrogen). Membranes were blocked with 5% BSA in PBS (blocking buffer) and incubated with primary antibodies diluted in blocking buffer. Membranes were washed and incubated with secondary antibodies diluted in blocking buffer. SuperSignal West Pico PLUS

Chemiluminescent Substrate (ThermoFisher #34579) was added on the membranes and pictures were taken on a myECL Imager (ThermoFisher).

Microscopy Immunolabeling and Imaging. 293T-ACE2 cells were cultured and infected with SARS-CoV-2 as described above. When indicated, cells were treated with 50 mg/mL of GRL-0617 (MedChemExpress #HY-117043), a specific inhibitor of SARS-CoV-2 PLpro (53), at the time of infection.
Cultures were rinsed with PBS and fixed with 4% paraformaldehyde (electronic microscopy grade; Alfa Aesar) in PBS for 10 min at room temperature, treated with 50 mM NH_4Cl for 10 min, permeabilized with 0.5% Triton X-100 for 15 min, and blocked with 0.3% BSA for 10 min. Cells were incubated with primary and secondary antibodies for 1h and 30 min, respectively, in a moist chamber. Nuclei were labeled with Hoechst dye (Molecular Probes). Images were acquired using a LSM700 (Zeiss) confocal microscope equipped with a 63X objective or by Airyscan LSM800 (Zeiss). Image analysis was performed using ImageJ.

Single-cell RNAseq analysis. Single cell RNAseq analysis were performed in the BioTuring Browser Software (v2.8.42) developed by BioTuring, using a dataset made available by Liao *et al.* (42) (ID: GSE145926). All processing steps were done by BioTuring Browser (62). Cells with less than 200 genes and mitochondrial genes higher than 10% were excluded from the analysis.

Statistical analysis. GraphPad Prism was used for statistical analyses. Linear models were computed using Rstudio.

Figures.

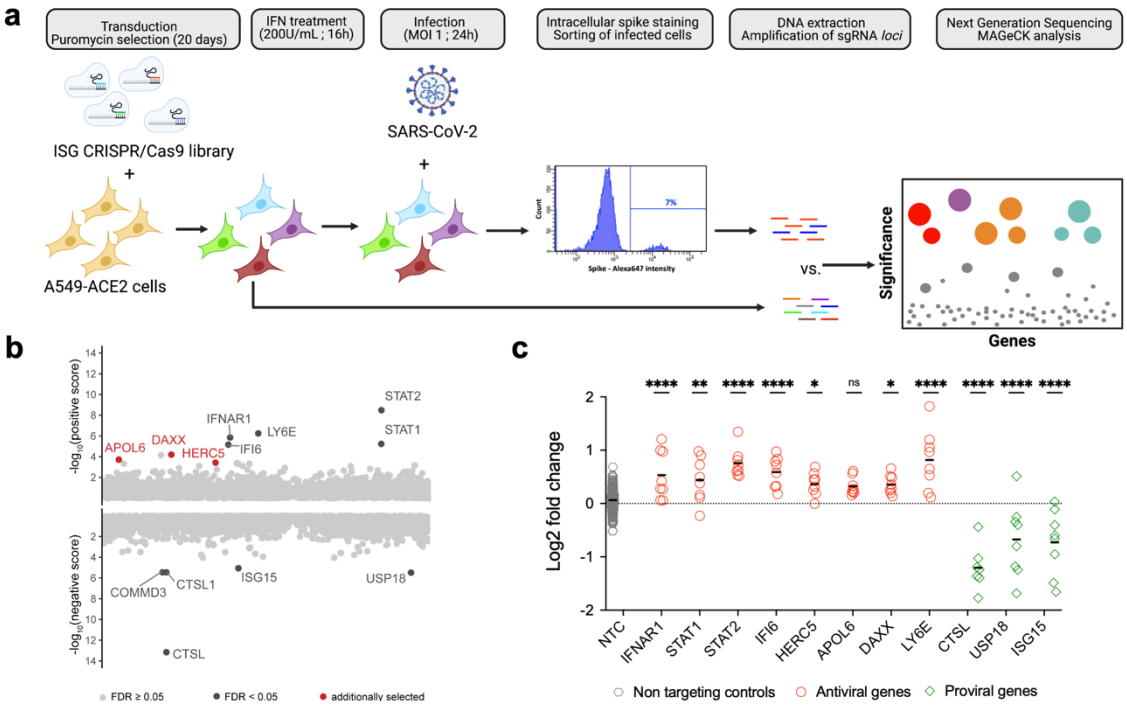

Figure 1: ISG-focused CRISPR/Cas9 screening approach to identify restriction factors for SARS-CoV-2. a: CRISPR/Cas9 screen outline. A549-ACE2 cells were transduced with lentivectors encoding the ISG CRISPR/Cas9 library and selected by puromycin treatment for 20 days. Library cells were then pre-treated with 200 U/mL of IFNα for 16 hours, and infection with SARS-CoV-2 at MOI 1. 24 hours post infection, infected cells were fixed with formalin treatment, permeabilized by saponin treatment and stained with a monoclonal anti-spike antibody. After secondary staining, infected cells were sorted and harvested. Non-infected, non-IFNα treated cells were harvested as a control. DNA was extracted from both cellular fractions and sgRNA *loci* amplification was carried out by PCR. Following NGS, bio-informatic analysis using the MAGeCK package was conducted. **b: Screen results**. By taking into account the enrichment ratios of each of the 8 different sgRNAs for every gene, the MAGeCK analysis provides a modified robust rank aggregation (α-RRA) score, with further one-sided significance testing. A positive score is assigned to KOs enriched in infected cells (*i.e.* restriction factor, represented in the top fraction of the graph) and a negative score is assigned to KOs depleted in infected cells (*i.e.* proviral factors, represented in the bottom portion of the graph). Gene with an FDR < 0.05 are represented in black. 3 genes with a FDR > 0.05, but with a p-value < 0.005 were additionally selected and are represented in red. **c: Individual sgRNA enrichment.** For the indicated genes, the enrichment ratio of the 8 sgRNAs present in the library was calculated as the MAGeCK normalized read counts in infected cells divided by those in the original pool of cells and is represented in log2 fold change. As a control, the enrichment ratios of the 200 non-targeting control sgRNAs (NTCs) are also represented, merged together in one NTC for visualization purposes only. Statistics: one-way ANOVA, ns = p-value > 0.05, * = p-value < 0.05, ** = p-value < 0.01, **** = p-value < 0.0001.

Table 1: Gene editing efficiency.

Gene	% of alleles edited
LY6E	97
DAXX	82
APOL6	99
HERC5	97
CTSL	87
IFI6	83
IFNAR1	79

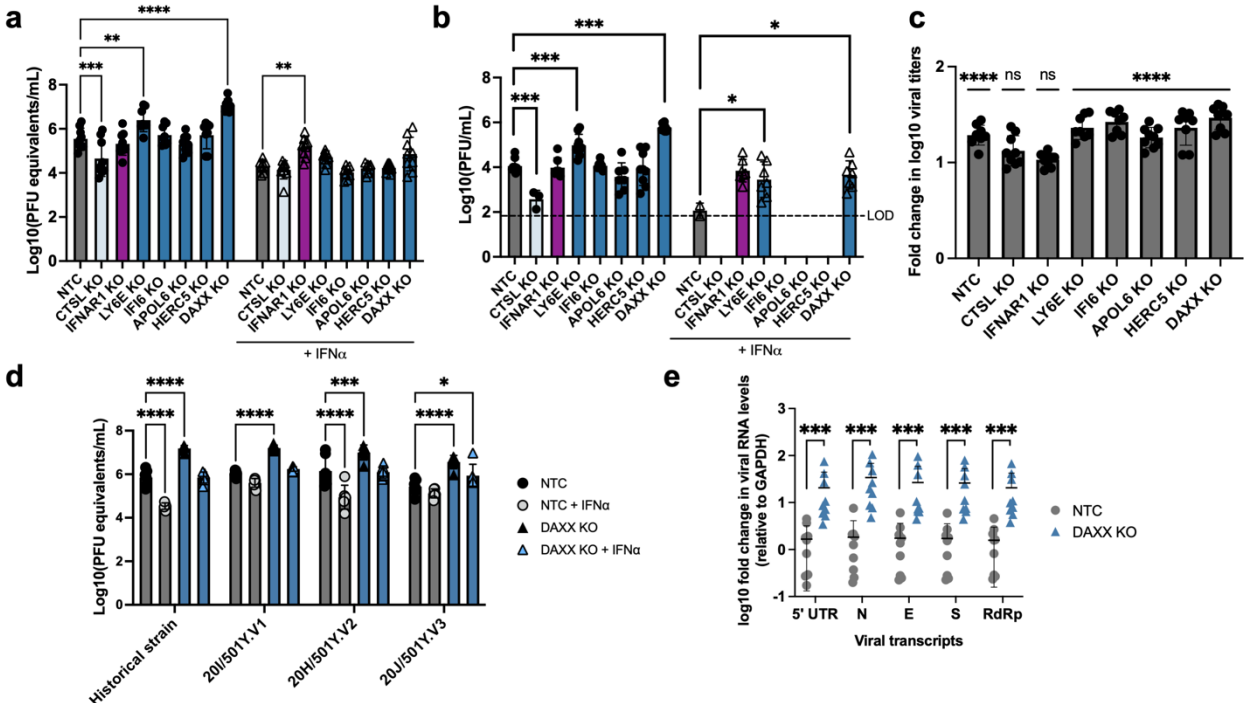

Figure 2: DAXX is a restriction factor for SARS-CoV-2. A-C: Antiviral activity of ISGs against SARS-CoV-2. A549-ACE2 knocked-out for the indicated genes were generated using a multi-guide approach, leading to pools of KO cells with a high frequency of indels. KO cells were pre-treated with 0 (circles) or 200 (triangles) U/mL of IFNα 24h prior to triplicate infection with SARS-CoV-2 (MOI 0.1). Supernatants were harvested at 72h post infection. The mean of three independent experiments, with infections carried out in triplicate, is shown. **a:** For the titration of RNA levels, supernatants were heat inactivated prior to quantification by qRT-PCR. Serial dilutions of a stock of known infectious titer was used as a standard (PFU equivalents/mL). Statistics: 2-way ANOVA, * = p-value < 0.05, ** = p-value < 0.01, *** = p-value < 0.001, **** = p-value < 0.0001. **b:** For the titration of infectious virus levels by plaque assay, supernatants were serially diluted and used to infect VeroE6 cells. Plaques formed after 3 days of infection were quantified using crystal violet coloration. Statistics: Dunnett's test on a linear model, * p-value < 0.05, ** p-value < 0.01, *** p-value < 0.001. **c:** For each of the indicated KO, the data shown in A is represented as fold change in log10 titers (*i.e.* the triplicate log10 titers of the non-treated condition divided by the mean of the triplicate log10 titers IFNα-treated condition, n=3). Statistics: 2-way ANOVA, ns = p-value > 0.05, **** = p-value < 0.001. **d:** A549-ACE2 WT or DAXX KO cells were infected in triplicates at an MOI of 0.1 with the following SARS-CoV-2 strains: BetaCoV/France/IDF0372/2020 (historical strain) ; hCoV-19/France/IDF-IPP11324/2020 (20I/501Y.V1, sometimes referred to as United Kingdom or B.1.1.7) ; hCoV-19/France/PDL-IPP01065/2021 (20H/501Y.V2, sometimes referred to as South Africa or B.1.351) ; hCoV-19/Japan/TY7-501/2021 (20J/501Y.V3, sometimes referred to as Brazil or P.1). Supernatants were harvested at 72h post infection. Supernatants were heat inactivated prior to quantification by qRT-PCR. Serial dilutions of a stock of known infectious titer was used as a standard (PFU equivalents/mL). The mean of two independent experiments, with infections carried out in triplicate, is shown. Statistics: 2-way ANOVA, * = p-value < 0.05, *** = p-value < 0.001, **** = p-value < 0.0001. **e:** A549-ACE2 WT or DAXX KO were infected in triplicates with SARS-CoV-2 at a MOI of 0.1. After 72h of infection, cell monolayers were harvested and cellular RNAs were extracted. The levels of each of the indicated viral transcripts were quantified by qRT-PCR and normalized to GAPDH levels. Fold change in DAXX KO cells compared to the average of control cells is represented. 3 independent experiments are shown and taken into account as fixed effects in a linear model. Statistics: Dunnett's test on a linear model, * p-value < 0.05, ** p-value < 0.01, *** p-value < 0.001.

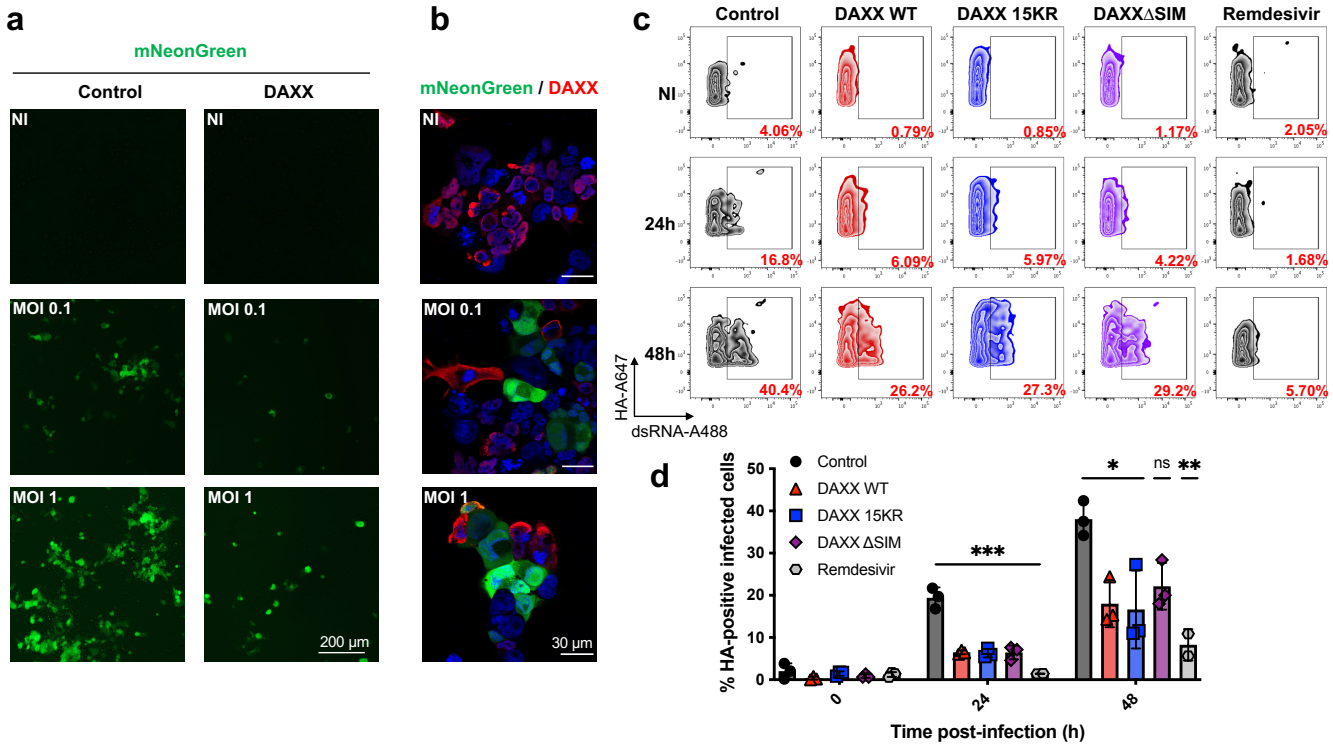

Figure 3: DAXX restriction of SARS-CoV-2 is SUMOylation independent. A-B: DAXX overexpression restricts SARS-CoV-2. 293T-ACE2 cells were transfected with DAXX WT. 24h after transfection, cells were infected with the mNeonGreen fluorescent reporter SARS-CoV-2 at the indicated MOI. Cells were either visualized with an EVOS fluorescence microscope (**a**) or stained with an HA-antibody detecting DAXX and imaged by confocal microscopy (**b**). Scale bars correspond to 200 µm (**a)** and 30 µm (**b**) **c-d: DAXX mutants are still able to restrict SARS-CoV-2**. 293T-ACE2 cells were transfected with HA-DAXX WT ; H-ADAXX 15KR ; HA-DAXXΔSIM ; or with HA-NRB1 as negative control plasmid. 24h after transfection, cells were infected with SARS-CoV-2 at an MOI of 0.1. When indicated, cells were treated with remdesivir at the time of infection. After 24 or 48h, infected cells were double-stained recognizing dsRNA (to read out infection) and HA (to read out transfection efficiency) and acquired by flow cytometry. The percentage of infected cells among HA-positive (transfected) cells for one representative experiments is shown in **c**, for the mean of 3 independent experiments in **d**. Statistics: one-way ANOVA Holm corrected, ns = p-value > 0.05, * = p-value < 0.05, ** = p-value < 0.01, *** = p-value < 0.001.

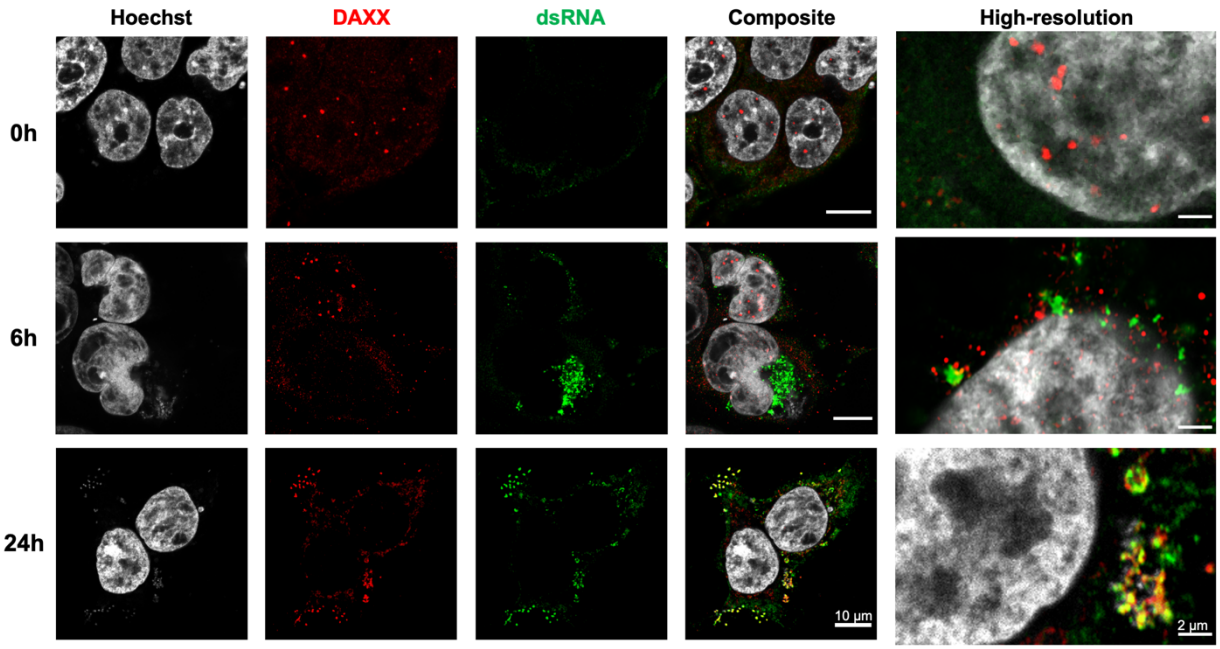

Figure 4: SARS-CoV-2 infection induces DAXX cytoplasmic re-localization to sites of viral replication. 293T-ACE2 cells were infected with SARS-CoV-2 at the indicated MOI 1. 24h post-infection, cells were labelled with Hoescht and with antibodies against dsRNA (detecting viral RNA, in green) and HA (detecting DAXX, in red). When indicated, the high-resolution Airyscan mode was used. Scale bars correspond to 10 µm for confocal images, and 2 µm for the high-resolution images.

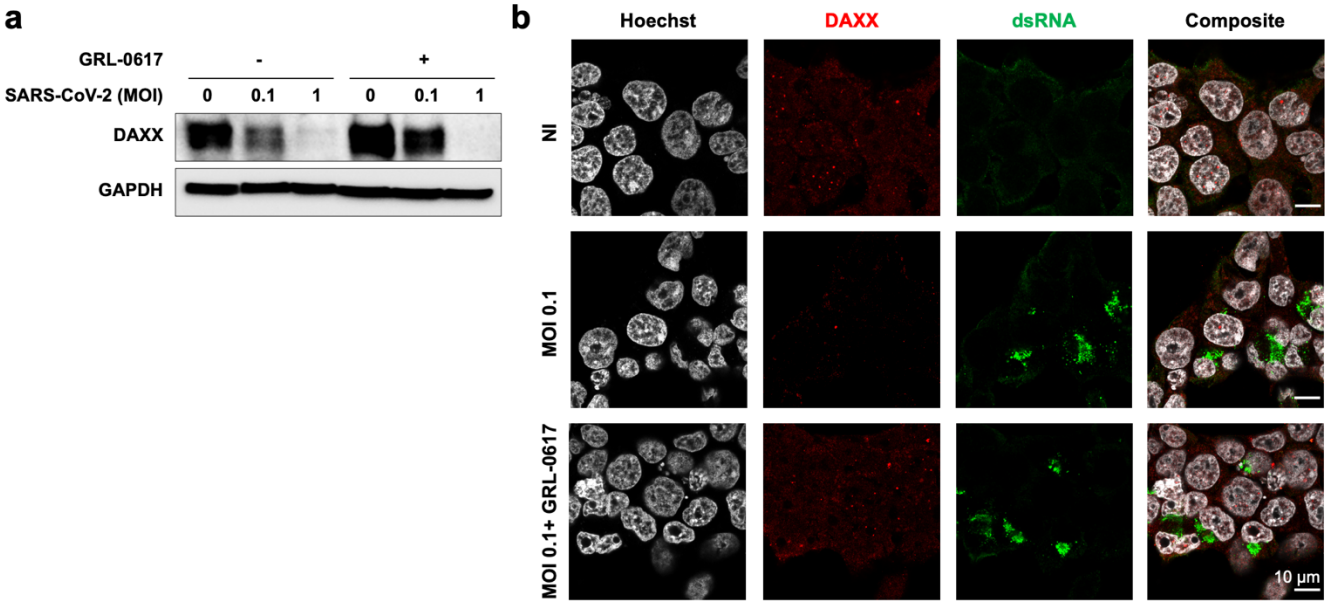

Figure 5: SARS-CoV-2 antagonizes DAXX restriction. a: DAXX degradation after infection. 293T-ACE2 cells were infected with SARS-CoV-2 at the indicated MOI. After 24h, cells were harvested and levels of DAXX and GAPDH were analyzed by Western Blot. When indicated, cells were treated with the viral protease inhibitor GRL-0617 at the time of infection. **b: GRL-0617 treatment partially reverses DAXX re-localization and expression.** 293T-ACE2 cells were infected with SARS-CoV-2 at the indicated MOI 0.1. 24h post-infection, cells were labelled with Hoescht and with antibodies against dsRNA (detecting viral RNA, in green) and HA (detecting DAXX, in red). When indicated, cells were treated with the viral protease inhibitor GRL-0617 at the time of infection. Scale bars correspond to 10 µm.

Acknowledgements. We thank the Cytometry Platform, Center for Technological Resources and Research, Institut Pasteur, for cell sorting experiments. This work was funded by the Institut Pasteur Coronavirus Task Force, CNRS (UMR 3569) and by the ANR (ANR-20-COVI-000, projects IDISCOVR to M.V. and Alpha-COV to S.N.). A.M.K. is supported by a grant of the French Ministry of Higher Education, Research and Innovation. G.M. is supported by a grant from the Agence nationale de recherches sur le sida et les hépatites virales (ANRS). We thank Michael Emerman, Daniel Marc and Ignacio Caballero-Posadas for helpful comments on the manuscript. Illustrative figures in this manuscript were created with BioRender.com.

Contributions. F.R. designed the research project. F.R. and M.V. secured the funding for the study. A.M.K., S.M.A., A.H., N.A., S.N., G.M., D.Q.T., M.C., T.V. and F.R. performed and analyzed the *in vitro* experiments. F.P. produced the stocks of lentivirus. J.C.S., J.O. and K.H. generated and validated KO cell lines. T.B. performed the single-cell RNAseq data analysis. A.B. and E.S.L. performed the bio-informatic analyses of the CRISPR/Cas9 screen. M.O., T.B., O.S., N.J., S.N., and M.V. analyzed the data and supervised the project. A.M.K. and F.R. wrote the manuscript. All authors edited the manuscript.

Competing Interests: J.C.S., J.O. and K.H. are employees and shareholders from Synthego Corporation.

Correspondence and requests for materials should be addressed to M.V. or F.R.

Data availability: Raw NGS data was deposited to the NCBI GEO portal and is accessible with the number GSE173418.

References.

1. Ruetsch C, Brglez V, Crémoni M, Zorzi K, Fernandez C, Boyer-Suavet S, et al. Functional Exhaustion of Type I and II Interferons Production in Severe COVID-19 Patients. Front Med. 2021 Jan 27;7:603961.
2. Hadjadj J, Yatim N, Barnabei L, Corneau A, Boussier J, Smith N, et al. Impaired type I interferon activity and inflammatory responses in severe COVID-19 patients. Science. 2020 Aug 7;369(6504):718–24.
3. Combes AJ, Courau T, Kuhn NF, Hu KH, Ray A, Chen WS, et al. Global absence and targeting of protective immune states in severe COVID-19. Nature. 2021 Mar 1;591(7848):124–30.
4. Blanco-Melo D, Nilsson-Payant BE, Liu W-C, Uhl S, Hoagland D, Møller R, et al. Imbalanced Host Response to SARS-CoV-2 Drives Development of COVID-19. Cell. 2020 May;181(5):1036-1045.e9.
5. Galani I-E, Rovina N, Lampropoulou V, Triantafyllia V, Manioudaki M, Pavlos E, et al. Untuned antiviral immunity in COVID-19 revealed by temporal type I/III interferon patterns and flu comparison. Nat Immunol. 2021 Jan;22(1):32–40.
6. Bastard P, Rosen LB, Zhang Q, Michailidis E, Hoffmann H-H, Zhang Y, et al. Autoantibodies against type I IFNs in patients with life-threatening COVID-19. Science. 2020 Oct 23;370(6515):eabd4585.
7. Zhang Q, Bastard P, Liu Z, Le Pen J, Moncada-Velez M, Chen J, et al. Inborn errors of type I IFN immunity in patients with life-threatening COVID-19. Science. 2020 Oct 23;370(6515):eabd4570.
8. Sa Ribero M, Jouvenet N, Dreux M, Nisole S. Interplay between SARS-CoV-2 and the type I interferon response. PLOS Pathog. 2020 Jul 29;16(7):e1008737.
9. Rebendenne A, Chaves Valadão AL, Tauziet M, Maarifi G, Bonaventure B, McKellar J, et al. SARS-CoV-2 Triggers an MDA-5-Dependent Interferon Response Which Is Unable To Control Replication in Lung Epithelial Cells. J Virol. 2021 Mar 25;95(8):e02415-20.

548 10. Yin X, Riva L, Pu Y, Martin-Sancho L, Kanamune J, Yamamoto Y, et al. MDA5 Governs the
549 Innate Immune Response to SARS-CoV-2 in Lung Epithelial Cells. Cell Rep. 2021 Jan;34(2):108628.
550 11. Felgenhauer U, Schoen A, Gad HH, Hartmann R, Schaubmar AR, Failing K, et al. Inhibition of
551 SARS–CoV-2 by type I and type III interferons. J Biol Chem. 2020 Oct 9;295(41):13958–64.
552 12. Lokugamage KG, Hage A, de Vries M, Valero-Jimenez AM, Schindewolf C, Dittmann M, et al.
553 Type I Interferon Susceptibility Distinguishes SARS-CoV-2 from SARS-CoV. J Virol. 2020 Nov
554 9;94(23):e01410-20.
555 13. Hoagland DA, Møller R, Uhl SA, Oishi K, Frere J, Golynker I, et al. Leveraging the antiviral
556 type I interferon system as a first line of defense against SARS-CoV-2 pathogenicity. Immunity. 2021
557 Jan;S1074761321000406.
558 14. Busnadiego I, Fernbach S, Pohl MO, Karakus U, Huber M, Trkola A, et al. Antiviral Activity of
559 Type I, II, and III Interferons Counterbalances ACE2 Inducibility and Restricts SARS-CoV-2. mBio.
560 2020 Oct 27;11(5):e01928-20.
561 15. Zhao X, Zheng S, Chen D, Zheng M, Li X, Li G, et al. LY6E Restricts Entry of Human
562 Coronaviruses, Including Currently Pandemic SARS-CoV-2. J Virol. 2020 Aug 31;94(18):e00562-20.
563 16. Pfaender S, Mar KB, Michailidis E, Kratzel A, Boys IN, V'kovski P, et al. LY6E impairs
564 coronavirus fusion and confers immune control of viral disease. Nat Microbiol. 2020 Nov;5(11):1330–
565 9.
566 17. Shi G, Kenney AD, Kudryashova E, Zani A, Zhang L, Lai KK, et al. Opposing activities of
567 IFITM proteins in SARS-CoV-2 infection. EMBO J. 2021 Feb 1;40(3):e106501.
568 18. Buchrieser J, Dufloo J, Hubert M, Monel B, Planas D, Rajah MM, et al. Syncytia formation by
569 SARS-CoV-2-infected cells. EMBO J. 2020 Dec;39(23).
570 19. Biering SB, Sarnik SA, Wang E, Zengel JR, Sathyan V, Nguyenla X, et al. Genome-wide,
571 bidirectional CRISPR screens identify mucins as critical host factors modulating SARS-CoV-2
572 infection. bioRxiv. 2021 Jan 1;2021.04.22.440848.
573 20. Nchioua R, Kmiec D, Müller JA, Conzelmann C, Groß R, Swanson CM, et al. SARS-CoV-2 Is
574 Restricted by Zinc Finger Antiviral Protein despite Preadaptation to the Low-CpG Environment in
575 Humans. mBio. 2020 Oct 27;11(5):e01930-20.
576 21. Martin-Sancho L, Lewinski MK, Pache L, Stoneham CA, Yin X, Becker ME, et al. Functional
577 Landscape of SARS-CoV-2 Cellular Restriction. Mol Cell. 2021 Apr 13;
578 22. Bonaventure B, Rebendenne A, Garcia de GF, McKellar J, Tauziet M, Chaves Valadão AL, et
579 al. A genome-wide CRISPR/Cas9 knock-out screen identifies the DEAD box RNA helicase DDX42 as
580 a broad antiviral inhibitor. bioRxiv. 2020 Jan 1;2020.10.28.359356.
581 23. Hoffmann H-H, Sánchez-Rivera FJ, Schneider WM, Luna JM, Soto-Feliciano YM, Ashbrook
582 AW, et al. Functional interrogation of a SARS-CoV-2 host protein interactome identifies unique and
583 shared coronavirus host factors. Cell Host Microbe. 2021 Feb;29(2):267-280.e5.
584 24. Daniloski Z, Jordan TX, Wessels H-H, Hoagland DA, Kasela S, Legut M, et al. Identification of
585 Required Host Factors for SARS-CoV-2 Infection in Human Cells. Cell. 2021 Jan;184(1):92-105.e16.
586 25. Wei J, Alfajaro MM, DeWeirdt PC, Hanna RE, Lu-Culligan WJ, Cai WL, et al. Genome-wide
587 CRISPR Screens Reveal Host Factors Critical for SARS-CoV-2 Infection. Cell. 2021 Jan;184(1):76-
588 91.e13.
589 26. Schneider WM, Luna JM, Hoffmann H-H, Sánchez-Rivera FJ, Leal AA, Ashbrook AW, et al.
590 Genome-Scale Identification of SARS-CoV-2 and Pan-coronavirus Host Factor Networks. Cell. 2021
591 Jan;184(1):120-132.e14.
592 27. Wang R, Simoneau CR, Kulsuptrakul J, Bouhaddou M, Travisano KA, Hayashi JM, et al.
593 Genetic Screens Identify Host Factors for SARS-CoV-2 and Common Cold Coronaviruses. Cell. 2021
594 Jan;184(1):106-119.e14.
595 28. Baggen J, Persoons L, Vanstreels E, Jansen S, Van Looveren D, Boeckx B, et al. Genome-wide
596 CRISPR screening identifies TMEM106B as a proviral host factor for SARS-CoV-2. Nat Genet. 2021

Apr;53(4):435–44.
29. Tang J, Wu S, Liu H, Stratt R, Barak OG, Shiekhattar R, et al. A novel transcription regulatory complex containing death domain-associated protein and the ATR-X syndrome protein. J Biol Chem. 2004 May 7;279(19):20369–77.
30. Porter SS, Stepp WH, Stamos JD, McBride AA. Host cell restriction factors that limit transcription and replication of human papillomavirus. Virus Res. 2017 Mar 2;231:10–20.
31. Maillet S, Fernandez J, Decourcelle M, El Koulali K, Blanchet FP, Arhel NJ, et al. Daxx Inhibits HIV-1 Reverse Transcription and Uncoating in a SUMO-Dependent Manner. Viruses. 2020 Jun 11;12(6).
32. Dutrieux J, Maarifi G, Portilho DM, Arhel NJ, Chelbi-Alix MK, Nisole S. PML/TRIM19-Dependent Inhibition of Retroviral Reverse-Transcription by Daxx. PLoS Pathog. 2015 Nov;11(11):e1005280.
33. OhAinle M, Helms L, Vermeire J, Roesch F, Humes D, Basom R, et al. A virus-packageable CRISPR screen identifies host factors mediating interferon inhibition of HIV. eLife. 2018 Dec 6;7:e39823.
34. Li W, Xu H, Xiao T, Cong L, Love MI, Zhang F, et al. MAGeCK enables robust identification of essential genes from genome-scale CRISPR/Cas9 knockout screens. Genome Biol. 2014 Dec 5;15(12):554.
35. Katopodis P, Anikin V, Randeva HS, Spandidos DA, Chatha K, Kyrou I, et al. Pan-cancer analysis of transmembrane protease serine 2 and cathepsin L that mediate cellular SARS-CoV-2 infection leading to COVID-19. Int J Oncol. 2020 Aug;57(2):533–9.
36. Malakhova OA, Yan M, Malakhov MP, Yuan Y, Ritchie KJ, Kim KI, et al. Protein ISGylation modulates the JAK-STAT signaling pathway. Genes Dev. 2003 Feb 15;17(4):455–60.
37. Broering R, Zhang X, Kottilil S, Trippler M, Jiang M, Lu M, et al. The interferon stimulated gene 15 functions as a proviral factor for the hepatitis C virus and as a regulator of the IFN response. Gut. 2010 Aug;59(8):1111–9.
38. McLaren PJ, Gawanbacht A, Pyndiah N, Krapp C, Hotter D, Kluge SF, et al. Identification of potential HIV restriction factors by combining evolutionary genomic signatures with functional analyses. Retrovirology. 2015 May 16;12:41.
39. Richardson RB, Ohlson MB, Eitson JL, Kumar A, McDougal MB, Boys IN, et al. A CRISPR screen identifies IFI6 as an ER-resident interferon effector that blocks flavivirus replication. Nat Microbiol. 2018 Nov;3(11):1214–23.
40. Merkl PE, Orzalli MH, Knipe DM. Mechanisms of Host IFI16, PML, and Daxx Protein Restriction of Herpes Simplex Virus 1 Replication. J Virol. 2018 May 15;92(10).
41. Jacquet S, Pontier D, Etienne L. Rapid Evolution of HERC6 and Duplication of a Chimeric HERC5/6 Gene in Rodents and Bats Suggest an Overlooked Role of HERCs in Mammalian Immunity. Front Immunol. 2020;11:605270.
42. Liao M, Liu Y, Yuan J, Wen Y, Xu G, Zhao J, et al. Single-cell landscape of bronchoalveolar immune cells in patients with COVID-19. Nat Med. 2020 Jun 1;26(6):842–4.
43. Haugh KA, Shalginskikh N, Nogusa S, Skalka AM, Katz RA, Balachandran S. The interferon-inducible antiviral protein Daxx is not essential for interferon-mediated protection against avian sarcoma virus. Virol J. 2014 May 28;11:100.
44. Guo K, Barrett BS, Mickens KL, Hasenkrug KJ, Santiago ML. Interferon Resistance of Emerging SARS-CoV-2 Variants. BioRxiv Prepr Serv Biol. 2021 Mar 21;
45. Maillet S, Nisole S. Daxx, a broad-spectrum viral restriction factor. Virol Montrouge Fr. 2016 Oct 1;20(5):261–72.
46. Kuo H-Y, Chang C-C, Jeng J-C, Hu H-M, Lin D-Y, Maul GG, et al. SUMO modification negatively modulates the transcriptional activity of CREB-binding protein via the recruitment of Daxx. Proc Natl Acad Sci U S A. 2005 Nov 22;102(47):16973–8.

646 47. Shih H-M, Chang C-C, Kuo H-Y, Lin D-Y. Daxx mediates SUMO-dependent transcriptional
647 control and subnuclear compartmentalization. Biochem Soc Trans. 2007 Dec;35(Pt 6):1397–400.
648 48. Sudharsan R, Azuma Y. The SUMO ligase PIAS1 regulates UV-induced apoptosis by
649 recruiting Daxx to SUMOylated foci. J Cell Sci. 2012 Dec 1;125(Pt 23):5819–29.
650 49. Jang M-S, Ryu S-W, Kim E. Modification of Daxx by small ubiquitin-related modifier-1.
651 Biochem Biophys Res Commun. 2002 Jul 12;295(2):495–500.
652 50. Lin D-Y, Huang Y-S, Jeng J-C, Kuo H-Y, Chang C-C, Chao T-T, et al. Role of SUMO-
653 interacting motif in Daxx SUMO modification, subnuclear localization, and repression of sumoylated
654 transcription factors. Mol Cell. 2006 Nov 3;24(3):341–54.
655 51. Xie X, Muruato A, Lokugamage KG, Narayanan K, Zhang X, Zou J, et al. An Infectious cDNA
656 Clone of SARS-CoV-2. Cell Host Microbe. 2020 May 13;27(5):841-848.e3.
657 52. Liu G, Lee J-H, Parker ZM, Acharya D, Chiang JJ, van Gent M, et al. ISG15-dependent
658 activation of the sensor MDA5 is antagonized by the SARS-CoV-2 papain-like protease to evade host
659 innate immunity. Nat Microbiol. 2021 Apr;6(4):467–78.
660 53. Shin D, Mukherjee R, Grewe D, Bojkova D, Baek K, Bhattacharya A, et al. Papain-like
661 protease regulates SARS-CoV-2 viral spread and innate immunity. Nature. 2020 Nov;587(7835):657–
662 62.
663 54. Saiz M, Martinez-Salas E. Uncovering targets of the Leader protease: Linking RNA-mediated
664 pathways and antiviral defense. Wiley Interdiscip Rev RNA. 2021 Feb 18;e1645.
665 55. Shaw AE, Hughes J, Gu Q, Behdenna A, Singer JB, Dennis T, et al. Fundamental properties of
666 the mammalian innate immune system revealed by multispecies comparison of type I interferon
667 responses. PLoS Biol. 2017 Dec 18;15(12):e2004086–e2004086.
668 56. Schreiner S, Bürck C, Glass M, Groitl P, Wimmer P, Kinkley S, et al. Control of human
669 adenovirus type 5 gene expression by cellular Daxx/ATRX chromatin-associated complexes. Nucleic
670 Acids Res. 2013 Apr 1;41(6):3532–50.
671 57. Guion LG, Sapp M. The Role of Promyelocytic Leukemia Nuclear Bodies During HPV
672 Infection. Front Cell Infect Microbiol. 2020;10:35.
673 58. Martin M. Cutadapt removes adapter sequences from high-throughput sequencing reads.
674 EMBnet.journal. 2011 May 2;17(1):10.
675 59. Langmead B, Salzberg SL. Fast gapped-read alignment with Bowtie 2. Nat Methods. 2012
676 Apr;9(4):357–9.
677 60. Li H, Handsaker B, Wysoker A, Fennell T, Ruan J, Homer N, et al. The Sequence
678 Alignment/Map format and SAMtools. Bioinforma Oxf Engl. 2009 Aug 15;25(16):2078–9.
679 61. Hsiau T, Conant D, Rossi N, Maures T, Waite K, Yang J, et al. Inference of CRISPR Edits from
680 Sanger Trace Data. bioRxiv. 2019 Jan 1;251082.
681 62. Le T, Phan T, Pham M, Tran D, Lam L, Nguyen T, et al. BBrowser: Making single-cell data
682 easily accessible. bioRxiv. 2020 Jan 1;2020.12.11.414136.